DOI: 10.1002/((please add manuscript number))

Article type: Communication

Compromising Charge Generation and Recombination with Asymmetric Molecule for High-performance Binary Organic Photovoltaics with Over 18% Certified Efficiency

Chengliang He, Zhaozhao Bi, Zeng Chen, Jing Guo, Xinxin Xia, Xinhui Lu, Jie Min, Haiming Zhu, Wei Ma, Lijian Zuo* and Hongzheng Chen**

C. He, Prof. L. Zuo, Prof. H. Chen

State Key Laboratory of Silicon Materials, MOE Key Laboratory of Macromolecular Synthesis and Functionalization, Department of Polymer Science and Engineering, Zhejiang University, 310027 Hangzhou, P. R. China.
E-mail: zjuzlj@zju.edu.cn, hzchen@zju.edu.cn

Z. Bi, Prof. W. Ma
State Key Laboratory for Mechanical Behavior of Materials, Xi' an Jiaotong University, Xi' an 710049, P. R. China.

E-mail: msewma@xjtu.edu.cn

Z. Chen, Prof. H. Zhu

Department of Chemistry, Zhejiang University, Hangzhou 310027, P. R. China.

J. Guo, Prof. J. Min

The Institute for Advanced Studies, Wuhan University, Wuhan 430072, P. R. China.

X. Xia, Prof. X. Lu

Department of Physics, Chinese University of Hong Kong, New Territories, Hong Kong 999077, P. R. China.

Prof. L. Zuo

Zhejiang University-Hangzhou Global Scientific and Technological Innovation Center, Hangzhou 310014, P. R. China.

Keywords: organic photovoltaic, bulk-heterojunction, asymmetric electron acceptor, charge generation, energy loss reduction

Balancing the charge generation and recombination constitutes a major challenge to break the current limit of organic photovoltaics (OPVs). To address this issue, we develop an asymmetric non-fullerene acceptor (NFA), namely the AC9, and demonstrate high-performance OPV with champion efficiency of 18.43% (18.1% certified). This represents the record value among binary OPVs. Comprehensive analysis on exciton dissociation, charge collection, carrier transport, and recombination have been carried out, unveiling that the improved device performance of asymmetric AC9 based OPVs is originated from a better compromise between charge generation and non-radiative charge recombination, compared to the corresponding symmetric ones. Our work provides a high-performing molecule and paves the way for high-performance OPVs through asymmetric molecular design.

As an emerging and appealing solar energy harvesting technology, organic photovoltaics (OPVs) are experiencing an encouraging era with a continuing breakthrough in power conversion efficiency (PCE), reaching certified results of over 18% for single-junction devices.[1-9] However, compared with inorganic solar

cells, the bulk heterojunction-based OPVs need extra energy to separate the tightly bound photoexcited electron-hole pairs, causing larger open-circuit voltage (V_{oc}) loss.[10] Generally, the OPVs have to sacrifice V_{oc} with large V_{oc} loss ranging from 0.6 eV to 1.1 eV to guarantee efficient charge generation, and this value is much higher than those of efficient inorganic solar cells.[5,11-13] As a result, compromising the charge generation and voltage loss is the key to improving the device performance of OPV. Notably, the V_{oc} loss is mainly induced due to the severe non-radiative charge recombination.[14-16]

The continuous innovation of electron acceptors has greatly contributed to the development of research on reducing energy loss without sacrificing charge separation efficiency.[17-20] Particularly, the design of the Y-series non-fullerene acceptors (NFAs), e.g. Y6, significantly boosted the PCE when paired with polymer donor PM6.[21] Compared with other type acceptors, e.g. $PC_{71}BM$, IT-4F, etc.,[22,23] the Y-series acceptors could maintain relatively deep highest occupied molecular orbital (HOMO) levels when narrowing optical bandgap owing to the electron-deficient central core.[5,6,21,24,25] This makes it possible to achieve a broadened photon to electron response (or the external quantum efficiency (EQE)) range. Researchers found that sizeable ionization energy (IE) offsets are needed for efficient charge transfer (CT) since energy level bending caused by the acceptors' quadrupole moments prevents efficient exciton-to-charge-transfer state conversion at low energetic offsets.[11] Interestingly, it is found that some Y6 based solar cells exhibit moderate charge recombination and efficient hole transfer process under a small HOMO offset,[19,26-29] possibly due to the large enough

quadrupole moments,[30] the long exciton lifetime,[26] the distinctive molecular packing and the well-organized morphology.[28] Besides, a small HOMO offset tends to increase the CT state energy or reduce the energy difference between CT and localized excited (LE) state to reduce the non-radiative loss.[16,31] As a result, high charge generation efficiency and low non-radiative charge recombination have been simultaneously achieved.

Recently, a high-performance NFA named BTP-eC9 was developed by Hou's group through chemical modification on Y6, including the halogen and alky chains optimization.[32] BTP-eC9 exhibits enhanced electron-transport property, which increases short-circuit current (J_{sc}) and fill factor (FF) simultaneously, and thus yielding a champion PCE of 17.8% and a certified value of 17.3% in binary OPVs based on PM6: BTP-eC9. In addition to the side chain and terminal group engineering, it was found that the asymmetric designs (in skeleton, end-groups, side-chains, etc.) enable the already efficient system to get a step further in performance.[33-36] The asymmetric design could be a practical way for further efficiency improvement, for it could fine-tune the absorption, energy level, molecular orientation, and stacking pattern reasonably, thus improving the device performance by boosting the charge collection and luminescence property.[20,34,36-39]

In this work, based on the above consideration, we adopt the symmetry breaking strategy to the state-of-the-art BTP-eC9 molecule *via* rational terminal selection. Terminals of IC-2Cl and CPTCN-Cl were utilized due to the consideration on energy level tuning and morphology control.[40,41] The IC-2Cl unit could enhance intramolecular charge transfer and intermolecular interaction, and it is also

found promising in energy loss reduction.[42] The CPTCN-Cl unit could promote V_{oc} effectively while guaranteeing high J_{sc} and FF.[41] Such terminal-asymmetry structure could be synthesized in fewer steps, preventing complicated synthetic routes of core-asymmetry. The resulting asymmetry acceptor (named AC9) can reach a record efficiency of 18.43% (18.1% certified) when blended with polymer donor PM6 (structure in **Figure 1b**), which is the highest among all asymmetric NFA based OPVs, and is also among the highest of certified binary OPVs so far. The CPTCN-Cl terminal substitution could enhance the electroluminescence quantum efficiency (EQE_{EL}) thus suppressing the non-radiative recombination loss.[43,44] Besides, the PM6:AC9 system features fast charge transfer based on the transient absorption spectroscopy (TAS) and transient photocurrent (TPC) results. Both efficient charge separation and low charge recombination could be achieved in PM6:AC9 based OPVs, and this enables realizing high J_{sc}, high $V_{oc,}$ and high FF simultaneously. This work provides a feasible approach to reduce energy loss while keeping charge separation efficient for high-performance OPVs.

The synthetic routes of the acceptors are depicted in **Scheme S1** and **Figures S1-S2.** We adopt the halogenated-thiophene-fused terminal (CPTCN-Cl) to replace the halogenated-benzene-fused one (IC-2Cl) due to its capacity in energy level tuning and morphology control.[41,44] The corresponding NFAs are developed by conjugating the end-groups to the BTP core via Knoevenagel condensation reaction. In the process of preparing and purifying AC9, we also obtain two by-products of BTP-eC9 and C9-2TC, the molar ratio is about 0.25:0.5:0.25 (BTP-eC9:AC9:C9-2TC). Detailed synthesis and molecular structure characterizations can be found in the

Supporting Information (**SI**). The three acceptors exhibit good solubility in common solvents such as chloroform and chlorobenzene.

The optical properties of the three acceptors were characterized by ultraviolet-visible (UV-vis) spectroscopy (**Figures 1c** and **S3**). BTP-eC9, AC9, and C9-2TC have similar maximal peaks located at 742 nm, 744 nm and 745 nm in chloroform solution, respectively. When converted into films, obvious red-shifts due to the strong intermolecular interactions could be observed. The maximal peak (831 nm) of AC9 neat film is between those of BTP-eC9 (834 nm) and C9-2TC (825 nm). Cyclic voltammetry was carried out to measure energy levels. The three acceptors exhibit up-shifted lowest unoccupied molecular orbital (LUMO) and HOMO levels accompanied with the introduction of CPTCN-Cl, as shown in **Figures 1d** and **S4**. The variation trend of energy levels is further confirmed by the ultraviolet photoelectron spectroscopy (UPS) measurement (**Figure S5**) and density functional theory (DFT) calculations based on the B3LYP/6-31G(d) level (**Figure S6**). The ionization potential differences were detected as 0.024 eV (BTP-eC9 and AC9) and 0.038 eV (BTP-eC9 and C9-2TC) from UPS tests. As shown in **Figure S6**, the calculated HOMO and LUMO levels show a trend consistent with the experimental data listed in **Figure 1d**. All of the three acceptors possess positive electrostatic potentials (ESPs), which could facilitate charge separation.[45] Based on the above results, we selected the wide bandgap polymer PM6 as the donor, which endows complementary absorption and suitable HOMO level offsets.

Devices with a conventional structure of ITO/PEDOT:PSS/Active Layer/PFN-Br/Ag were fabricated to characterize the photovoltaic properties. The detailed device

fabrication and characterizations are provided in **SI**. **Figure 2a** shows the current density-voltage (*J-V*) curves of OPVs based on PM6:BTP-eC9, PM6:AC9 and PM6:C9-2TC blends. Their photovoltaic parameters are summarized in **Table 1**. **Figure 2b** shows the PCE statistics of 30 cells for each blend. PM6:BTP-eC9 based champion device delivers a PCE of 18.11%, with a V_{oc} of 0.848 V, a very high J_{sc} of 26.90 mA cm^{-2} and a FF of 0.80. While, the PM6:C9-2TC based device exhibits a superior V_{oc} of 0.886 V but inferior J_{sc} (25.50 mA cm^{-2}) and FF (0.75), resulting in a relatively lower PCE of 16.89%, which could be ascribed to the insufficient charge transfer and obvious carrier recombination caused by the narrowed energy offsets as discussed below. Encouragingly, the PM6:AC9 based device exhibits a J_{sc} of 26.75 mA cm^{-2}, a FF of 0.79 and a V_{oc} of 0.871 V. This yields a champion PCE of 18.43% (a certified PCE of 18.1%). It is worthy to note that this is one of the best PCE among binary OPVs, and ranks the highest among OPVs with asymmetry structures (**Figure S7**). EQE tests were carried out and the results are displayed in **Figure 2c** and **Table 1**. The integrated J_{cal} values from the EQE curves are 26.45 mA cm^{-2}, 26.20 mA cm^{-2} and 25.18 mA cm^{-2} for OPVs based on PM6:BTP-eC9, PM6:AC9 and PM6:C9-2TC, respectively, close to those derived from their *J-V* curves. All of the three blends possess over 80% photon to electron response from 500 nm to 800 nm. Among the three acceptors, BTP-eC9 based device exhibits the highest J_{cal}, while C9-2TC based device shows the highest V_{oc}. Considering AC9 based device has a close J_{cal} to the BTP-eC9 based device as well as a high V_{oc} close to that of C9-2TC based one, it is argued that the highest PCE of PM6:AC9 based device is attributed to the better balance between charge generation (J_{sc}) and electron potential (V_{oc}).

Further investigations were conducted to probe the energy loss (E_{loss}) of these OPVs. The energy bandgap (E_g) is calculated from the EQE curve based on the method developed by Rau *et al.* (**Figures 2d** and **S8**, details see **Section 5** in **SI**),[46,47] and numerical values are 1.403 eV, 1.410 eV and 1.421 eV for PM6:BTP-eC9, PM6:AC9 and PM6:C9-2TC, respectively. Fourier transform photocurrent spectroscopy external quantum efficiency (FTPS-EQE) and electroluminescence quantum efficiency (EQE_{EL}) experiments were performed (**Figures 2e** and **2f**) and the detailed E_{loss} data are summarized in **Table 2** and **Figure 2h** (calculation methods are described in **Section 5** in **SI**). There is no big difference in the charge recombination from inevitable black body radiation (ΔE_1) and the non-ideal radiative decay (ΔE_2) among the three blends, due to their similar band gap and band tails. Usually, in disordered semiconductors, the co-existence of different localized states could extend the band tail absorption and cause the energetic disorder.[12] The Urbach energy (E_U) could characterize the degree of the energetic disorder caused by structural peculiarities as well as that induced by external factors.[48] The values of E_U are obtained from the FTPS-EQE curves by an exponential fit.[12] The calculated E_U (**Figure S11**) values are 24.6 meV, 24.1 meV and 24.7 meV for PM6:BTP-eC9, PM6:AC9 and PM6:C9-2TC blends, respectively. The difference of E_U is negligible, indicating that the asymmetric structure does not bring more disorder. The E_{loss} difference mainly originates from non-radiative decay (ΔE_3). ΔE_3 is calculated from the EQE_{EL} curves as shown in **Figures 2f** and **S9**. The slightly narrowed energy offset due to the introduction of the CPTCN-Cl terminal is beneficial to increase the CT-LE coupling for improving the luminescence properties,[31] leading to mitigated non-radiative recombination loss. In addition, we performed

electroluminescence (EL) tests based on the structure of ITO/PEDOT:PSS/Pure acceptor/PFN-Br/Ag (**Figure S10**). Obviously, the asymmetric AC9 shows the highest EL intensity under the same injection currents, and thus the highest EQE_{EL} among the three acceptors (**Figure 2g**). The high luminescence property of asymmetric AC9 will be of great help to reduce the non-radiative decay for low V_{oc} loss. Moreover, this result indicates that the asymmetric NFA molecule might possess the advantage of lower non-radiative charge recombination over the symmetric ones. As a result, the E_{loss} continuously decreases in sequence of PM6:BTP-eC9 (0.555 eV), PM6:AC9 (0.539 eV), and PM6:C9-2TC (0.535 eV). The PM6:AC9 based OPV exhibits E_{loss} closer to PM6:C9-2TC, as consistent with the V_{oc} variation.

Further, the charge transfer or separation was examined within the PM6:BTP-eC9, PM6:AC9, and PM6:C9-2TC blend films, *via* femtosecond TAS. The excitation wavelength of 800 nm was used here to selectively excite the acceptors in the D:A blends. As shown in **Figures 3a-3f** and **S12**, the bleaching signals located at ~840 nm could be naturally ascribed to the acceptor from their absorption profiles. The bleaching signal located at ~640 nm should be attributed to the PM6.[49] After excitation, it is clear that the signal located at ~640 nm increases significantly after the signal located at ~840 nm, suggesting the hole transfer from acceptors to polymer donor PM6 in all of the three blends (**Figures 3d-3f**). By extracting the kinetics (**Figure 3g**), the exciton dissociation and diffusion rates are numerically studied.[49] By utilizing a bi-exponential fitting, PM6:BTP-eC9 blend yields lifetimes of τ_1 = 0.29 ps and τ_2 = 10.8 ps, similar in the PM6:AC9 blend as τ_1 = 0.32 ps and τ_2 = 9.8 ps. The PM6:C9-2TC blend exhibits the lifetimes of τ_1=

0.25 ps and τ_2 = 10.10 ps. It is clear that the three systems exhibit very small difference in hole transfer, possibly due to the small HOMO offset differences within the three systems.[50] In addition, we calculated the hole transfer efficiency (HTE) of three PM6:NFA blends via ultrafast HT process and diffusion mediated HT process (method in **SI**, **Section 6**) from **Figure S13**,[49] which are 92.6%, 94.2%, 93.6% for PM6:BTP-eC9, PM6:AC9, PM6:C9-2TC blends, respectively (**Table S4**). All of the three blends show high HTE with small HOMO offset. Notably, the HTE of PM6:AC9 blend is most efficient, in well agreement with the best performance. We conducted TAS measurement onto μs time scale (**Figure S14**) to investigate the charge recombination, and find that the results show negligible difference. Therefore, we performed the transient photovoltage (TPV)/TPC test further (discussed hereafter) as a better supplement for the amplification of the difference.

To investigate the charge behaviors after charge separation, we studied the charge transiting process via TPC measurement further.[51] The TPC results (438 ns, 344 ns and 367 ns for PM6:BTP-eC9, PM6:AC9 and PM6:C9-2TC blends, respectively) show that the PM6:AC9 system possesses the shortest charge transiting time (**Figure 3h**), indicating the efficient charge extraction process, which is a complicate result of molecular packing, frontier molecular orbitals, interfacial contact, etc. Thus, the asymmetric molecule is conducive to promoting charge transport and facilitating carrier extraction, thereby maintaining high J_{sc} and FF.

The relationship between photocurrent density (J_{ph}) and effective voltage (V_{eff}) of the devices was studied to investigate the bias-dependent charge separation and

collection behavior (**Figure S15**). The exciton dissociation efficiency (P_{diss}) and charge collection efficiency (P_{coll}) could be calculated from the J_{ph}/J_{sat} values under short circuit and maximal power output conditions, respectively, where J_{sat} refers to the saturation current at a high V_{eff} ($V_{eff} \geq 2$ V). P_{diss} and P_{coll} are observed as 98.94% and 88.99% for PM6:AC9 blend, respectively, which are comparable to those of PM6:BTP-eC9 blend (P_{diss} ~ 99.45%, P_{coll} ~ 90.73%) but much higher compared to those of PM6:C9-2TC blend. The high exciton dissociation and collection efficiencies for the PM6:AC9 blend are consistent with the TPC results.

Further, the charge recombination kinetics process was examined. We firstly performed TPV measurements to investigate the charge recombination dynamics of the devices (**Figure 3i**). The test results show that the photo-carrier lifetime for PM6:BTP-eC9, PM6:AC9 and PM6:C9-2TC systems are 5.50 μs, 5.56 μs and 5.13 μs, respectively, indicating that PM6:AC9 system has the least charge recombination, which is consistent with the brightest electroluminescence of pristine AC9 film. Charge recombination behavior was then investigated by employing J-V properties as a function of light intensity (P_{light}). The relationship between V_{oc} and P_{light} could be described as $V_{oc} \propto nkT/q\ln(P_{light})$ (k is the Boltzmann constant, T is the temperature and q is the elementary charge, larger n value means more component of monomolecular recombination). As shown in **Figure S15**, the slope values of all the three blends approach kT/q, demonstrating that the dominant recombination in the active layer is the bimolecular recombination. The correlation between J_{sc} and P_{light} could be described as $J_{sc} \propto P_{light}^{\alpha}$ (the closer α value is to 1, the less component of bimolecular recombination exists). The α values are 0.994, 1.000 and

0.998 for PM6:BTP-eC9, PM6:AC9 and PM6:C9-2TC blends, respectively, indicating mitigated bimolecular recombination or efficient charge generation in all these systems, as consistent with the TAS measurement. The molecular asymmetric provides a solid way to compromise the benefits from both charge separation promotion and energy loss reduction for high-performance OPVs.

Grazing-incidence wide-angle and small-angle X-ray scattering (GIWAXS/GISAXS) characterizations were carried out to study the morphological factor of the three NFAs (**Figures 4** and **S16-S19**).[52-55] For the pristine acceptor films, strong signal peaks at q_z = ~1.74 Å^{-1} (d = ~3.61 Å) in the out-of-plane (OOP) direction and at q_r = ~0.401 Å^{-1} (d = ~15.7 Å) in the in-plane (IP) direction could be observed, indicating a dominant face-on orientated molecular stacking. Detailed parameters of peak intensity profiles along with IP/OOP direction are summarized in **Tables S5-S6**. Through the intensity profiles of the pure acceptor films, it can be found that the asymmetric AC9 possesses the highest peak signal intensity in both of the OOP and IP directions (**Figures S16** and **S17**), indicating its strong crystallinity to a certain extent, which is beneficial to the charge transport in acceptor phase. This enhanced crystallinity was also observed in other asymmetric acceptors.[34] From the coherence length (CL) values of the lamellar packing in the IP direction, it can be inferred that BTP-eC9 pristine film is less amorphous than others. However, this trend becomes very weak in their blend films. The π-π stacking (peaks at q_z = 1.74 Å^{-1} (d = 0.361 Å)) difference in the OOP direction is negligible, and the CL values of IP scatting peaks at q_r = 0.380 Å^{-1} (d = 16.5 Å) are 59 Å, 56 Å and 48 Å for PM6:BTP-eC9, PM6:AC9 and PM6:C9-2TC blends,

respectively. While in the out-of-plane direction, the π-π stacking difference is negligible. **Figure 4d** shows the GISAXS intensity profiles. Here, the scattering contribution from the pure acceptor phase is fitted by the fractal-like network model. The Debye-Anderson-Brumberger (DAB) model is used to account for the scattering due to the amorphous intermixing region.[54] The crystal domain sizes ($2R_g$) of the three blends are similar (25 nm-32 nm). Detailed data are summarized in **Table S7**. The IC-2Cl terminal and CPTCN-Cl terminal exhibit comparable ability in phase separation control.

In summary, we have developed a new NFA, i.e. the AC9, featuring an asymmetric structure based on the high-performance BTP-eC9. By substituting the IC-2Cl unit with the CPTCN-Cl unit in terminal capping, the asymmetric AC9 exhibits slightly blue-shifted absorption and decreased crystallinity but up-shifted energy levels. Moreover, the PM6:AC9 based OPV exhibits comparable charge separation and collection ability but much enhanced luminescence property for V_{oc} loss suppression, compared with PM6:BTP-eC9 based OPV. As a result, PM6:AC9 based OPVs exhibit a better compromise between charge recombination and generation, that is, a V_{oc} improvement while maintaining high J_{sc} and FF, thus achieving a record high PCE of 18.43% (certified 18.1%). This work demonstrates that asymmetric terminal design is a feasible strategy to realize charge separation promotion and energy loss reduction simultaneously for high-performance OPVs.

Supporting Information

Supporting Information is available from the Wiley Online Library or the author.

Acknowledgments

This work was supported by the National Natural Science Foundation of China (Nos. 21734008, 61721005, 52173185), National Key Research and Development Program of China (Nos. 2019YFA0705900, 2017YFA0207700), and Research Start-up Fund from Zhejiang University. X-ray data was acquired at beamlines 7.3.3 at the Advanced Light Source, which is supported by the Director, Office of Science, Office of Basic Energy Sciences, of the U.S. Department of Energy under Contract No. DE-AC02-05CH11231. The authors thank Chenhui Zhu at beamline 7.3.3 for assistance with data acquisition. The authors also thank Jianlong Xia and Kangwei Wang in Wuhan University of Technology for assistance with ns-μs TA data acquisition.

Received: ((will be filled in by the editorial staff))

Revised: ((will be filled in by the editorial staff))

Published online: ((will be filled in by the editorial staff))

References

[1] O. Inganas, *Adv. Mater.* **2018**, *30*, 1800388.

[2] J. Hou, O. Inganas, R. H. Friend, F. Gao, *Nat. Mater.* **2018**, *17*, 119.

[3] P. Cheng, G. Li, X. Zhan, Y. Yang, *Nat. Photonics* **2018**, *12*, 131.

[4] C. Yan, S. Barlow, Z. Wang, H. Yan, A. K. Y. Jen, S. R. Marder, X. Zhan, *Nat. Rev. Mater.* **2018**, *3*, 18003.

[5] J. Yuan, H. Zhang, R. Zhang, Y. Wang, J. Hou, M. Leclerc, X. Zhan, F. Huang, F. Gao, Y. Zou, Y. Li, *Chem* **2020**, *6*, 2147.

[6] S. Li, C.-Z. Li, M. Shi, H. Chen, *ACS Energy Lett.* **2020**, *5*, 1554.

[7] L. Zhan, S. Li, T.-K. Lau, Y. Cui, X. Lu, M. Shi, C.-Z. Li, H. Li, J. Hou, H. Chen, *Energy Environ. Sci.* **2020**, *13*, 635.

[8] L. Liu, S. Chen, Y. Qu, X. Gao, L. Han, Z. Lin, L. Yang, W. Wang, N. Zheng, Y. Liang, Y. Tan, H. Xia, F. He, *Adv. Mater.* **2021**, *33*, 2101279.

[9] NREL, Best Research-Cell Efficiencies, https://www.nrel.gov/pv/cell-efficiency.html.

[10] T. M. Clarke, J. R. Durrant, *Chem. Rev.* **2010**, *110*, 6736.

[11] S. Karuthedath, J. Gorenflot, Y. Firdaus, N. Chaturvedi, C. S. P. De Castro, G. T. Harrison, J. I. Khan, A. Markina, A. H. Balawi, T. A. D. Pena, W. Liu, R. Z. Liang, A. Sharma, S. H. K. Paleti, W. Zhang, Y. Lin, E. Alarousu, D. H. Anjum, P. M. Beaujuge, S. De Wolf, I. McCulloch, T. D. Anthopoulos, D. Baran, D. Andrienko, F. Laquai, *Nat. Mater.* **2021**, *20*, 378.

[12] S. Liu, J. Yuan, W. Deng, M. Luo, Y. Xie, Q. Liang, Y. Zou, Z. He, H. Wu, Y. Cao, *Nat. Photonics* **2020**, *14*, 300.

[13] J. Liu, S. Chen, D. Qian, B. Gautam, G. Yang, J. Zhao, J. Bergqvist, F. Zhang, W. Ma, H. Ade, O. Inganäs, K. Gundogdu, F. Gao, H. Yan, *Nat. Energy* **2016**, *1*, 16089.

[14] J. Yao, T. Kirchartz, M. S. Vezie, M. A. Faist, W. Gong, Z. He, H. Wu, J. Troughton, T. Watson, D. Bryant, J. Nelson, *Phys. Rev. Appl.* **2015**, *4*, 014020.

[15] J. Benduhn, K. Tvingstedt, F. Piersimoni, S. Ullbrich, Y. Fan, M. Tropiano, K. A. McGarry, O. Zeika, M. K. Riede, C. J. Douglas, S. Barlow, S. R. Marder, D. Neher, D. Spoltore, K. Vandewal, *Nat. Energy* **2017**, *2*, 17053.

[16] X.-K. Chen, D. Qian, Y. Wang, T. Kirchartz, W. Tress, H. Yao, J. Yuan, M. Hülsbeck, M. Zhang, Y. Zou, Y. Sun, Y. Li, J. Hou, O. Inganäs, V. Coropceanu, J.-L. Bredas, F. Gao, *Nat. Energy* **2021**, *6*, 799.

[17] S. Li, L. Zhan, C. Sun, H. Zhu, G. Zhou, W. Yang, M. Shi, C. Z. Li, J. Hou, Y. Li, H. Chen, *J. Am. Chem. Soc.* **2019**, *141*, 3073.

[18] K. Zhou, Y. Liu, A. Alotaibi, J. Yuan, C. Jiang, J. Xin, X. Liu, B. A. Collins, F. Zhang, W. Ma, *ACS Energy Lett.* **2020**, *5*, 589.

[19] C. Sun, S. Qin, R. Wang, S. Chen, F. Pan, B. Qiu, Z. Shang, L. Meng, C. Zhang, M. Xiao, C. Yang, Y. Li, *J. Am. Chem. Soc.* **2020**, *142*, 1465.

[20] S. Li, L. Zhan, Y. Jin, G. Zhou, T. K. Lau, R. Qin, M. Shi, C. Z. Li, H. Zhu, X. Lu, F. Zhang, H. Chen, *Adv. Mater.* **2020**, 2001160.

[21] J. Yuan, Y. Zhang, L. Zhou, G. Zhang, H.-L. Yip, T.-K. Lau, X. Lu, C. Zhu, H. Peng, P. A. Johnson, M. Leclerc, Y. Cao, J. Ulanski, Y. Li, Y. Zou, *Joule* **2019**, *3*, 1140.

[22] M. Zhang, X. Guo, W. Ma, H. Ade, J. Hou, *Adv. Mater.* **2015**, *27*, 4655.

[23] S. Zhang, Y. Qin, J. Zhu, J. Hou, *Adv. Mater.* **2018**, *30*, 1800868.

[24] C. He, Y. Li, Y. Liu, Y. Li, G. Zhou, S. Li, H. Zhu, X. Lu, F. Zhang, C.-Z. Li, H. Chen, *J. Mater. Chem. A* **2020**, *8*, 18154.

[25] C. He, Y. Li, S. Li, Z. P. Yu, Y. Li, X. Lu, M. Shi, C. Z. Li, H. Chen, *ACS Appl. Mater. Interfaces* **2020**, *12*, 16700.

[26] A. Classen, C. L. Chochos, L. Lüer, V. G. Gregoriou, J. Wortmann, A. Osvet, K. Forberich, I. McCulloch, T. Heumüller, C. J. Brabec, *Nat. Energy* **2020**, *5*, 711.

[27] A. Karki, J. Vollbrecht, A. L. Dixon, N. Schopp, M. Schrock, G. N. M. Reddy, T. Q. Nguyen, *Adv. Mater.* **2019**, *31*, 1903868.

[28] G. Zhang, X. K. Chen, J. Xiao, P. C. Y. Chow, M. Ren, G. Kupgan, X. Jiao, C. C. S. Chan, X. Du, R. Xia, Z. Chen, J. Yuan, Y. Zhang, S. Zhang, Y. Liu, Y. Zou, H. Yan, K. S. Wong, V. Coropceanu, N. Li, C. J. Brabec, J. L. Bredas, H. L. Yip, Y. Cao, *Nat. Commun.* **2020**, *11*, 3943.

[29] M. Zhang, L. Zhu, G. Zhou, T. Hao, C. Qiu, Z. Zhao, Q. Hu, B. W. Larson, H. Zhu, Z. Ma, Z. Tang, W. Feng, Y. Zhang, T. P. Russell, F. Liu, *Nat. Commun.* **2021**, *12*, 309.

[30] L. Perdigon-Toro, H. Zhang, A. Markina, J. Yuan, S. M. Hosseini, C. M. Wolff, G. Zuo, M. Stolterfoht, Y. Zou, F. Gao, D. Andrienko, S. Shoaee, D. Neher, *Adv. Mater.* **2020**, *32*, 1906763.

[31] D. Qian, Z. Zheng, H. Yao, W. Tress, T. R. Hopper, S. Chen, S. Li, J. Liu, S. Chen, J. Zhang, X. K. Liu, B. Gao, L. Ouyang, Y. Jin, G. Pozina, I. A. Buyanova, W. M. Chen, O. Inganas, V. Coropceanu, J. L. Bredas, H. Yan, J. Hou, F. Zhang, A. A. Bakulin, F. Gao, *Nat. Mater.* **2018**, *17*, 703.

[32] Y. Cui, H. Yao, J. Zhang, K. Xian, T. Zhang, L. Hong, Y. Wang, Y. Xu, K. Ma, C. An, C. He, Z. Wei, F. Gao, J. Hou, *Adv. Mater.* **2020**, *32*, 1908205.

[33] W. Gao, H. Fu, Y. Li, F. Lin, R. Sun, Z. Wu, X. Wu, C. Zhong, J. Min, J. Luo, H. Y. Woo, Z. Zhu, A. K. Y. Jen, *Adv. Energy Mater.* **2020**, *11*, 2003141.

[34] S. Li, L. Zhan, N. Yao, X. Xia, Z. Chen, W. Yang, C. He, L. Zuo, M. Shi, H. Zhu, X. Lu, F. Zhang, H. Chen, *Nat. Commun.* **2021**, *12*, 4627.

[35] Y. Chen, F. Bai, Z. Peng, L. Zhu, J. Zhang, X. Zou, Y. Qin, H. K. Kim, J. Yuan, L. K. Ma, J. Zhang, H. Yu, P. C. Y. Chow, F. Huang, Y. Zou, H. Ade, F. Liu, H. Yan, *Adv. Energy Mater.* **2020**, *11*, 2007231.

[36] C. Li, H. Fu, T. Xia, Y. Sun, *Adv. Energy Mater.* **2019**, *9*, 1900999.

[37] L. Zhan, S. Li, X. Xia, Y. Li, X. Lu, L. Zuo, M. Shi, H. Chen, *Adv. Mater.*

2021, *33*, 2007231.

[38] W. Gao, X. Ma, Q. An, J. Gao, C. Zhong, F. Zhang, C. Yang, *J. Mater. Chem. A* **2020**, *185*, 108970.

[39] H. Chen, H. Lai, Z. Chen, Y. Zhu, H. Wang, L. Han, Y. Zhang, F. He, *Angew. Chem. Int. Ed.* **2021**, *60*, 3238.

[40] Y. Cui, C. Yang, H. Yao, J. Zhu, Y. Wang, G. Jia, F. Gao, J. Hou, *Adv. Mater.* **2017**, *29*, 1703080.

[41] Z. Luo, T. Liu, Y. Wang, G. Zhang, R. Sun, Z. Chen, C. Zhong, J. Wu, Y. Chen, M. Zhang, Y. Zou, W. Ma, H. Yan, J. Min, Y. Li, C. Yang, *Adv. Energy Mater.* **2019**, *9*, 1900041.

[42] Y. Cui, H. Yao, J. Zhang, T. Zhang, Y. Wang, L. Hong, K. Xian, B. Xu, S. Zhang, J. Peng, Z. Wei, F. Gao, J. Hou, *Nat. Commun.* **2019**, *10*, 2515.

[43] Z. Luo, R. Ma, T. Liu, J. Yu, Y. Xiao, R. Sun, G. Xie, J. Yuan, Y. Chen, K. Chen, G. Chai, H. Sun, J. Min, J. Zhang, Y. Zou, C. Yang, X. Lu, F. Gao, H. Yan, *Joule* **2020**, *4*, 1.

[44] W. Yang, Z. Luo, R. Sun, J. Guo, T. Wang, Y. Wu, W. Wang, J. Guo, Q. Wu, M. Shi, H. Li, C. Yang, J. Min, *Nat. Commun.* **2020**, *11*, 1218.

[45] H. Yao, Y. Cui, D. Qian, C. S. Ponseca, Jr., A. Honarfar, Y. Xu, J. Xin, Z. Chen, L. Hong, B. Gao, R. Yu, Y. Zu, W. Ma, P. Chabera, T. Pullerits, A. Yartsev, F. Gao, J. Hou, *J. Am. Chem. Soc.* **2019**, *141*, 7743.

[46] U. Rau, B. Blank, T. C. M. Müller, T. Kirchartz, *Phys. Rev. Appl.* **2017**, *7*, 044016.

[47] Y. Wang, D. Qian, Y. Cui, H. Zhang, J. Hou, K. Vandewal, T. Kirchartz, F. Gao, *Adv. Energy Mater.* **2018**, *8*, 1801352.

[48] F. Urbach, *Phys. Rev.* **1953**, *92*, 1324.

[49] Z. Chen, X. Chen, B. Qiu, G. Zhou, Z. Jia, W. Tao, Y. Li, Y. M. Yang, H. Zhu, *J. Phys. Chem. Lett.* **2020**, *11*, 3226.

[50] Z. Chen, X. Chen, Z. Jia, G. Zhou, J. Xu, Y. Wu, X. Xia, X. Li, X. Zhang, C. Deng, Y. Zhang, X. Lu, W. Liu, C. Zhang, Y. Yang, H. Zhu, *Joule* **2021**, *5*, 1.

[51] L. Liu, Y. Kan, K. Gao, J. Wang, M. Zhao, H. Chen, C. Zhao, T. Jiu, A. K. Jen, Y. Li, *Adv. Mater.* **2020**, *32*, 1907604.

[52] A. Hexemer, W. Bras, J. Glossinger, E. Schaible, E. Gann, R. Kirian, A.

MacDowell, M. Church, B. Rude, H. Padmore, *J. Phys.: Conference Series* **2010**, *247*.

[53] L. Zhang, B. Lin, B. Hu, X. Xu, W. Ma, *Adv. Mater.* **2018**, *30*, 1800343.

[54] J. Mai, Y. Xiao, G. Zhou, J. Wang, J. Zhu, N. Zhao, X. Zhan, X. Lu, *Adv. Mater.* **2018**, *8*, 1802888.

[55] L. Zhang, X. Xu, B. Lin, H. Zhao, T. Li, J. Xin, Z. Bi, G. Qiu, S. Guo, K. Zhou, X. Zhan, W. Ma, *Adv. Mater.* **2018**, *30*, 1805041.

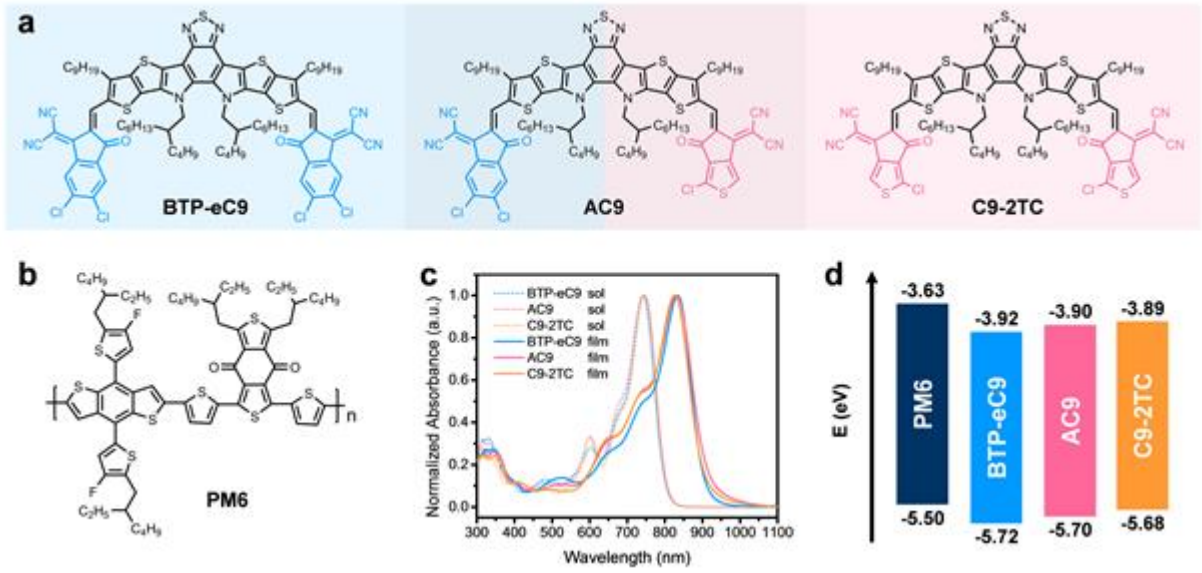

Figure 1. Chemical structures of a) NFAs of BTP-eC9, AC9, and C9-2TC and b) polymer donor PM6. c) UV-vis absorption spectra of the pristine acceptors in films and $CHCl_3$ solutions. d) Energy level diagram determined by cyclic voltammetry.

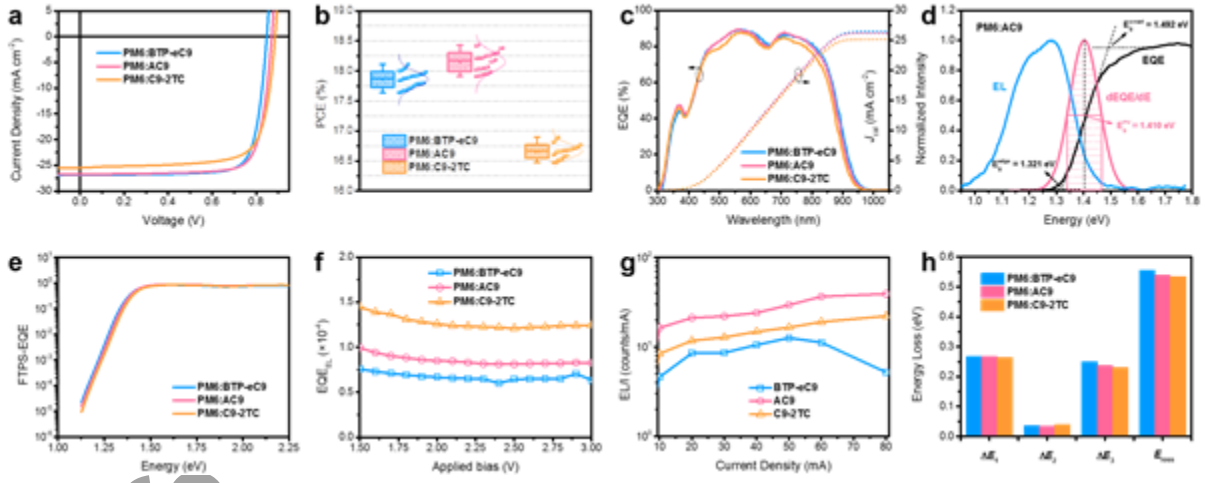

Figure 2. a) *J*–*V* curves of the optimal devices. b) PCE statistics of 30 cells for each blend. c) EQE curves of the optimal devices. d) E_g determination method based on EQE curve and EL curve. e) FTPS-EQE curves and f) EQE_{EL} curves of the optimal devices. g) EQE_{EL} curves of the pristine acceptor films. h) Comparison of energy loss in the three types of devices.

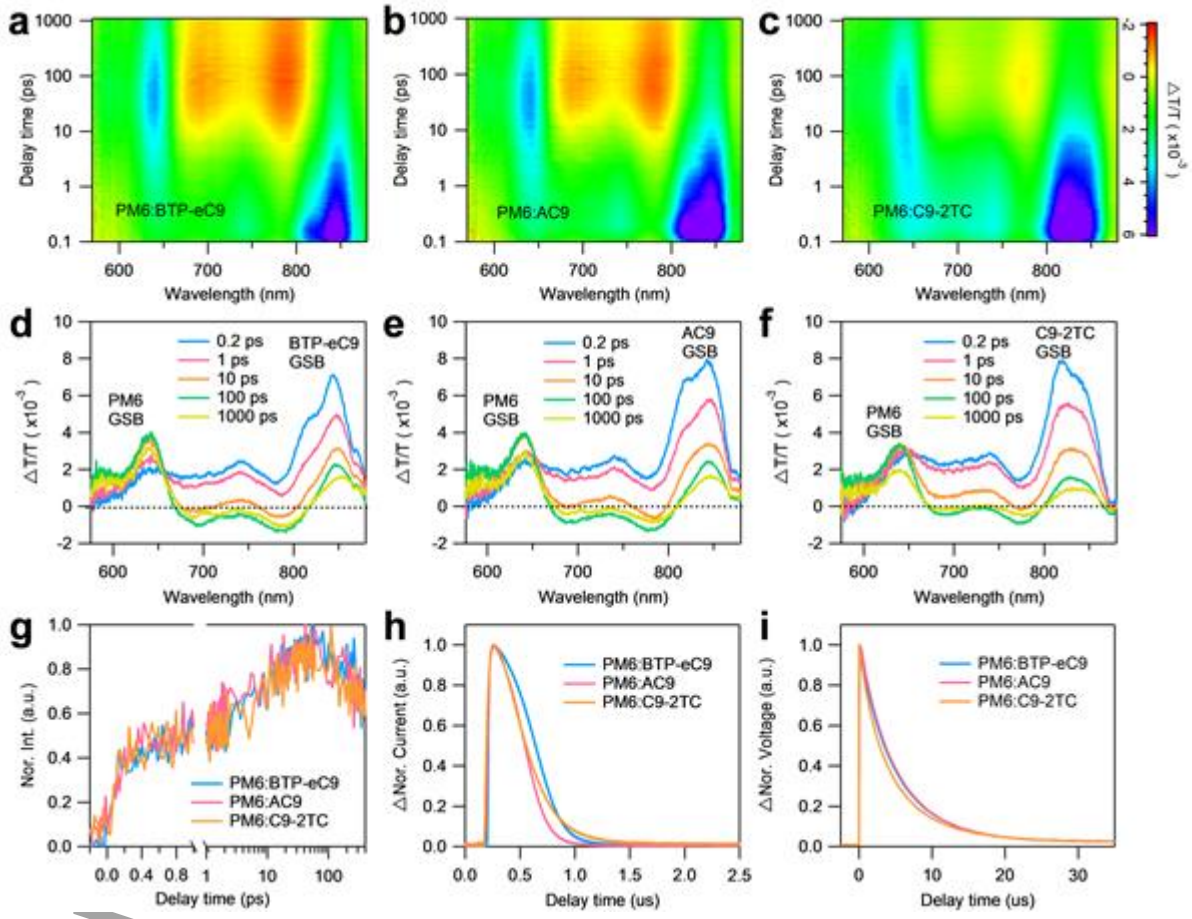

Figure 3. Color plots of the TA spectra of a) PM6:BTP-eC9 blend, b) PM6:AC9 blend and c) PM6:C9-2TC blend under 800 nm excitation. TA spectra of d) PM6:BTP-eC9 blend, e) PM6:AC9 blend and f) PM6:C9-2TC blend excited at 800 nm at different delay times. g) Hole transfer dynamic curves of the three blends. h) Normalized transient photocurrent traces of the optimal devices. i) Normalized transient photovoltage traces of the optimal devices.

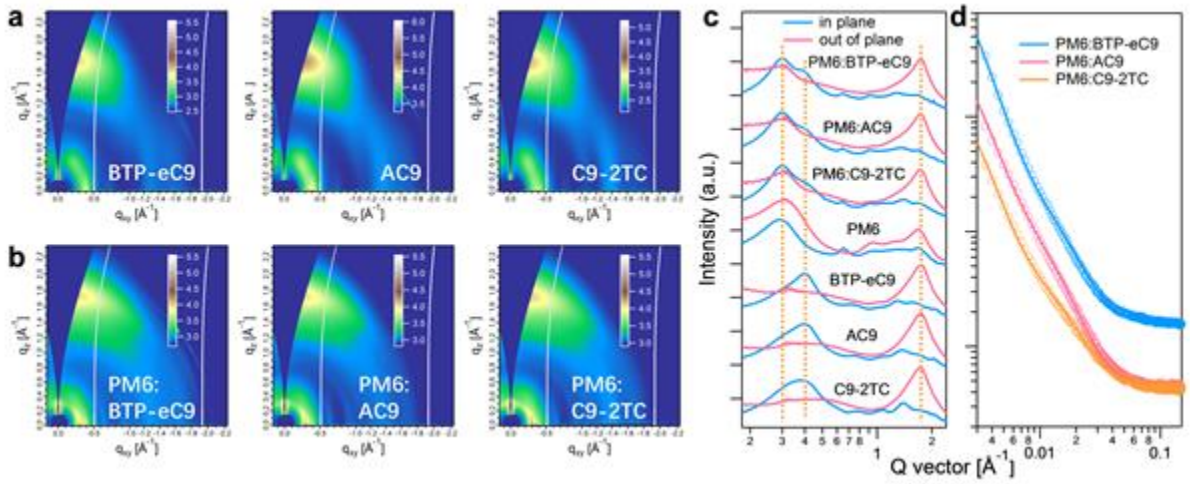

Figure 4. 2D GIWAXS images of a) pristine acceptor films and b) blend films. c) GIWAXS intensity profiles of the corresponding films along the in-plane (blue lines) and out-of-plane (red lines) directions. d) GISAXS intensity profiles of the corresponding films along the q_r axis.

Table 1. Photovoltaic parameters of OPVs based on different small molecule acceptors.

Active Layer	V_{oc} (V)	J_{sc} (mA cm^{-2})	J_{cal} (mA cm^{-2}) [a]	FF	PCE (%) [b]
PM6:BTP-eC9	0.848 (0.850±0.003)	26.90 (26.65±0.18)	26.45	0.80 (0.79±0.01)	18.11 (17.86±0.13)
PM6:AC9	0.871 (0.869±0.002)	26.75 (26.57±0.16)	26.20	0.79 (0.79±0.00)	18.43 (18.15±0.16)
PM6:C9-2TC	0.886 (0.884±0.002)	25.50 (25.42±0.32)	25.18	0.75 (0.74±0.01)	16.89 (16.66±0.11)
PM6:AC9	0.867	26.75	¥	0.78	18.1 [c]

[a] Integrated current densities from EQE curves.

[b] Average PCEs from 30 devices.

[c] Certified by the National Institute of Metrology (NIM), China.

Table 2. Detailed energy loss of OPVs based on different small molecule acceptors.

Active layer	E_g^{PV} (eV)	qV_{oc} (eV)	E_{loss} (eV)	qV_{oc}^{SQ} (eV)	qV_{oc}^{rad} (eV)	ΔE_1 (eV)	ΔE_2 (eV)	ΔE_3 (eV)	EQE_{EL}	Exp. $q\Delta V_{oc}^{non-rad}$ (eV)
PM6:BTP-eC9	1.403	0.848	0.555	1.136	1.099	0.267	0.037	0.251	6.42×10^{-5}	0.249
PM6:AC9	1.410	0.871	0.539	1.143	1.109	0.267	0.034	0.238	8.16×10^{-5}	0.243
PM6:C9-	1.421	0.886	0.535	1.156	1.116	0.265	0.040	0.230	$1.24\times10^{-}$	0.232

Asymmetric electron acceptor AC9 was designed and synthesized by different end-groups. Devices based on PM6:AC9 achieved high charge generation efficiency and low non-radiative charge recombination simultaneously, yielding a champion efficiency of 18.43% (certified 18.1%). This is one of the best efficiency among binary organic photovoltaics, and ranks the highest among organic photovoltaics with asymmetry acceptors.

organic photovoltaic, bulk-heterojunction, asymmetric electron acceptor, charge generation promotion, energy loss reduction

Chengliang He, Zhaozhao Bi, Zeng Chen, Jing Guo, Xinxin Xia, Xinhui Lu, Jie Min, Haiming Zhu, Wei Ma*, Lijian Zuo* and Hongzheng Chen*

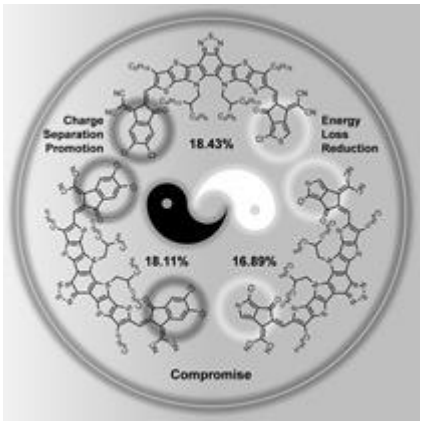

Compromising Charge Generation and Recombination with Asymmetric Molecule for High-performance Binary Organic Photovoltaics with Over 18% Certified Efficiency